Supporting Information for

Slightly Li-enriched chemistry enabling super stable $LiNi_{0.5}Mn_{0.5}O_2$ cathodes under extreme conditions

Siqi Chen[a], Ping Zhang[a], Xin Zhou[a], Wenbin Wu[a], Xiaohong Liu[a,*], Yifeng Liu[b], Guilin Feng[c], Bin Zhang[d], Wangyan Xing[d], Meihua Zuo[d], Ping Zhang[d], Genpin Lv[e], Yao Xiao[b,*], Shixue Dou[f], Wei Xiang[a,g,*]

[a] *College of Materials and Chemistry & Chemical Engineering, Chengdu University of Technology, Chengdu 610059, Sichuan, China.*

[b] *College of Chemistry and Materials Engineering, Wenzhou University, Wenzhou, 325035, PR China.*

[c] *Research Institute of Frontier Science, Southwest Jiaotong University, Chengdu 610031, PR China.*

[d] *Yibin Libode New Materials Co., Ltd. Yibin 644200, PR China.*

[e] *Ruyuan HEC New Energy Materials Co., Ltd., Ruyuan 512700, PR China.*

[f] *Institute of Energy Materials Science, University of Shanghai for Science and Technology, Shanghai 200093, PR China.*

[g] *Tianfu Yongxing Laboratory, Chengdu 610213, PR China.*

Corresponding author: xiangwei@cdut.edu.cn (Wei Xiang); xiaoyao@wzu.edu.cn (Yao Xiao); xhl@cdut.edu.cn (Xiaohong Liu)

1. Experimental section

1.1 Synthesis of cathodes

The pristine, W doped, and Li_2WO_4-modified $LiNi_{0.5}Mn_{0.5}O_2$ layered oxide cathodes were synthesized by high temperature solid-phase method using co-precipitated $Ni_{0.5}Mn_{0.5}(OH)_2$ as precursor. For the synthesis of pristine $LiNi_{0.5}Mn_{0.5}O_2$ (NM50), stoichiometric $Ni_{0.5}Mn_{0.5}(OH)_2$ and $LiOH{\cdot}H_2O$ (99.99%) were mixed in an agate mortar, with anhydrous ethanol as solvent and the molar ratio between Li and TM is 1.06. The mixture was placed in a muffle furnace, pre-burned at 550 ℃ for 6 h, and then heated to 750 ℃ for 12 hours in air atmosphere with a heating rate of 3 ℃ min^{-1}. For the synthesis of (1-*x*)$LiNi_{0.5}Mn_{0.5}O_2{\cdot}xLi_2WO_4$ (*x*=0, 0.01, 0.02, 0.03, 0.05; and denoted as NM50-LW1, NM50-LW2, NM50-LW3 and NM50-LW5, respectively), similar procedure was used as the synthesis of NM50 except for the addition of different amount of WO_3 and corresponding excess LiOH according the molecular formula of Li_2WO_4 to compensate the Li loss and promote the formation of Li_2WO_4. Take $0.98LiNi_{0.5}Mn_{0.5}O_2{\cdot}0.02Li_2WO_4$ as example, the mole ratio between Li and M (M=Ni, Mn, W) is 1.0812. For the synthesis of 2 mol% W doped $LiNi_{0.49}Mn_{0.49}W_{0.02}O_2$ (NM50-W2) cathode, similar procedure was used as the synthesis of NM50 except for the addition of 2 mol% WO_3 during mixing, and the ratio between Li and M (M=Ni, Mn, W) is 1.06. For the synthesis of 2 mol% WO_3 coated $0.98LiNi_{0.5}Mn_{0.5}O_2{\cdot}0.02WO_3$ (NM50-WO2) cathode, stoichiometric amount of $LiNi_{0.5}Mn_{0.5}O_2$ and WO_3 (99%) were mixed in an agate mortar with ethanol as solvent and then placed in a muffle furnace at 750 ℃ in air atmosphere for 4 h.

1.2 Material characterization

The crystal structure of the cathodes was determined by X-ray diffraction (XRD, Rigaku, Japan), where the test target was Cu target Kα radiation source, the scan speed was 2° min^{-1}, the scan angle was 10°-80°, and the test voltage and current were 40 kV and 40 mA. The Rietveld refinement of the diffraction data was performed by Jade 6.0 and GSAS/EXPGUI programs to obtain phase structure and crystal information. The morphology and structure of the particles were observed by scanning electron microscopy (SEM, FESEM, FEI QUANTA 250). The lattice fringe electron diffraction pattern and microstructure of the cathodes were observed by transmission electron microscopy (TEM, FEI Talos F200S, USA). The high-resolution TEM (HRTEM) images were analyzed and processed by Digital Micrograph software to obtain fast Fourier transform (FFT) images. The element distribution of Ni, Mn and W elements of the cathodes was detected by energy dispersive X-ray spectroscopy (EDS). The valence states of the element were tested by X-ray photoelectron spectroscopy (XPS) of Thermo Scientific K-Alpha, USA. All spectra were calibrated to the

peak of the C-C peak in C1*s* (284.8 eV). Operando XRD was performed in transmission mode at a constant current density of 10 mA g^{-1}. The charged cathodes (with cut-off voltage of 4.5 V) were measured by differential scanning calorimetry (DSC) using a DSC214 in the range of 50 to 450 ℃ at a temperature scanning rate of 5 ℃ min^{-1}. For DSC analysis, the coin battery was charged at a rate of C/10 to 4.5 V vs. Li/Li^+. The electrode was obtained in an Ar-filled glove box and washed carefully with diethyl carbonate (DEC) solvent. The cathode material was then scraped off from the collector and placed on an Aluminum plate with slightly fresh electrolyte for testing. The O_2 and CO_2 produced from the cathodes in Ar carrier gas was determined at a flow rate of 0.9 mL min^{-1} using an in-situ differential electrochemical mass spectrometer (DEMS-QMG220, Zero Dew Instrument Shanghai Co., Ltd.). Quantitative gas evolution data on the 32 (O_2) and 44 (CO_2) m/z channels were collected, and the DEMS battery was charged at a rate of 0.1 C (20 mA g^{-1}) to 4.5 V.

1.3 Electrochemical test

The cathode active material was mixed with carbon black (Super-P) and polyvinylidene fluoride (with mass ratio of 80:10:10) in N-methylpyridine (NMP) to prepare the slurry using an agate mortar. The obtained homogeneous slurry was coated on aluminum foil using a plate coating machine (MSK-AFA-HC100) with coating thickness of 150 mm and dried in a vacuum oven at 105 °C for 12 h. Then the electrodes were pressed with a roller press under a constant load of 4.6 KN. The loading amount of active material on the disc with a diameter of 14 mm was 3-4 mg $\cdot$ cm^{-2}. The semi-cell test was performed with a coin-type CR2025 battery, which consisted of the prepared cathode, separator, lithium metal anode and an appropriate amount of electrolyte, where the electrolyte consisted of 1.2 mol L^{-1} $LiPF_6$ in a mixture of vinyl carbonate (EC) and dimethyl carbonate (DMC) (with volume ratio of 1:1). The CR2025 battery was assembled in an Ar-filled glove box (H_2O < 0.01 ppm, O_2 < 0.01 ppm). The battery test system (LANDdt-CT2001A, China) was used to conduct the electrochemical test in potential range of 2.7-4.5 V and 2.7-4.6 V (1 C = 170 mAh g^{-1}), at 30 and 55 °C at a constant current. The long-term cycling performance of the cathodes was also evaluated using a full cell assembled with separator, and electrolyte (a 1.2M LiPF6 dissolved in ethyl carbonate/dimethyl carbonate (EC: DMC=1:1 by volume)) and graphite in the potential range of 2.7-4.5 V at a current of 1 C at 30 ℃. And the loading mass of active material in full cells is about 9.3 mg cm^{-2}. Each cathode was tested at least three times to ensure reliability. The electrochemical impedance spectroscopy (EIS) test was performed using an electrochemical workstation (CHI 660D) to study the reaction kinetics of the electrode. The test frequency range was 100 ~ 0.01 Hz, and the test data were fitted and analyzed using Zview software. The lithium-ion diffusion coefficient during the charge-discharge process was determined by the galvanostatic

intermittent titration technique (GITT). The test was conducted in the potential range of 2.7-4.5 V at 0.1 C, the current application time was 30 min, and the intermittent time was 60 min. The lithium-ion diffusion was calculated using the following formula:

$$D_{Li+} = \frac{4}{\pi\tau}\left(\frac{m_B V_M}{M_B S}\right)^2 \left(\frac{\Delta E_s}{\Delta E_\tau}\right)^2 (\Delta\tau << L^2/D)$$

τ (s) is the time of constant current charging, m_B (g) is the mass of the active substance, V_M is the molar volume of the sample ($cm^3\ mol^{-1}$), M_B ($g\ cm^{-1}$) is the molar mass of the sample, S (cm^2) is the area of the electrode, ΔE_S (V) is the steady-state voltage difference, ΔE_τ (V) is the value of charging or discharging at time τ when a constant current I_0 is applied, and L (cm) is the diffusion length.

2. Supporting Figures and text

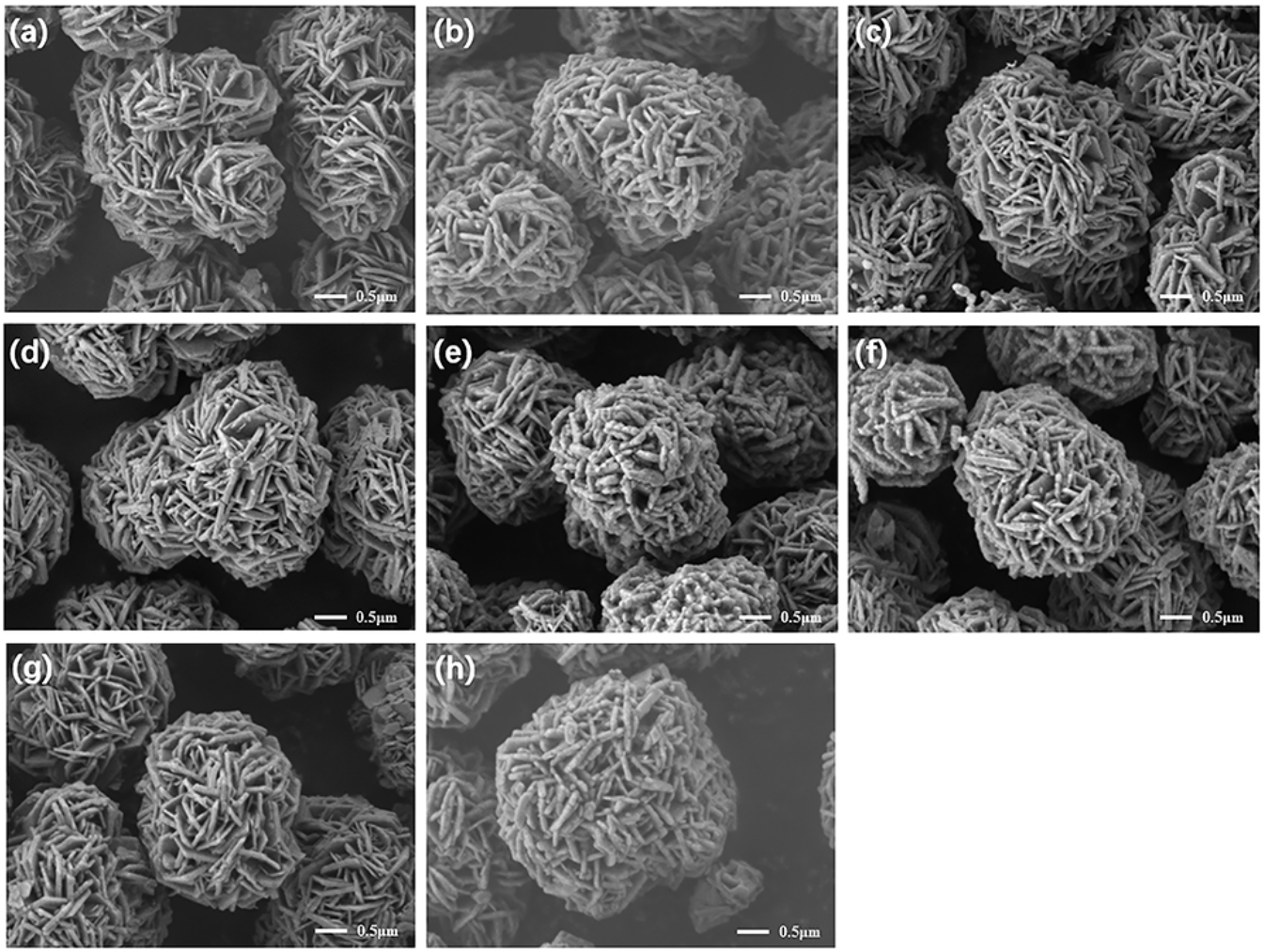

Fig. S1 SEM images of $Ni_{0.5}Mn_{0.5}(OH)_2$ (a), NM50 (b), NM50-LW1(c), NM50-LW2 (d), NM50-LW3 (e), NM50-LW5 (f), NM50-W2 (g) and NM50-WO2 (h).

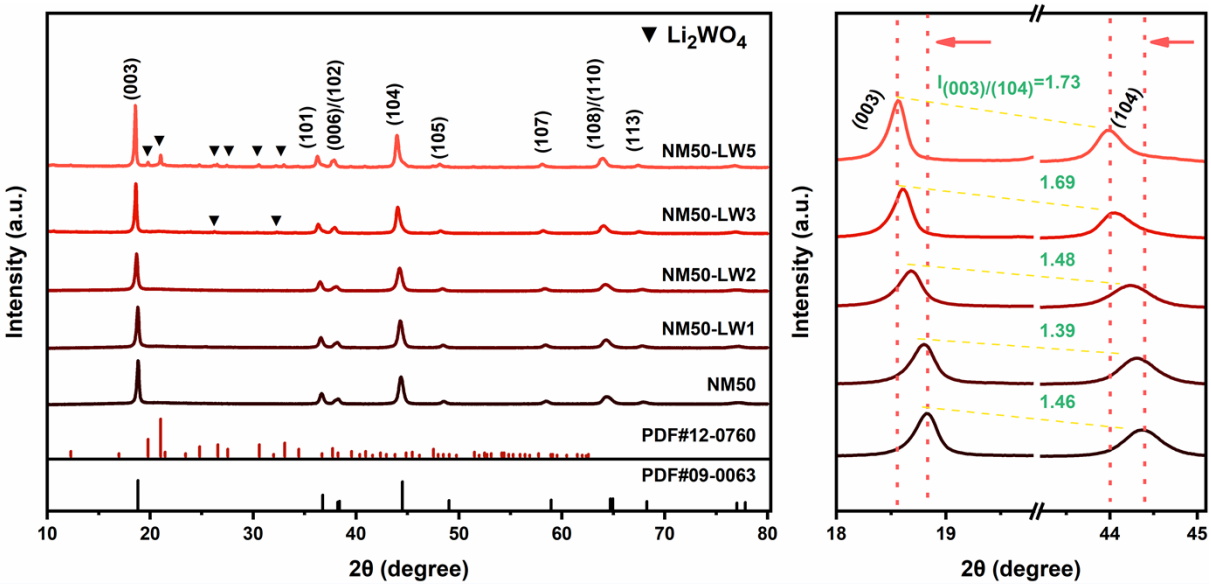

Fig. S2 (a) XRD pattern and the corresponding enlarged (003) and (104) peaks of NM50, NM50-LW1, NM50-LW2, NM50-LW3 and NM50-LW5.

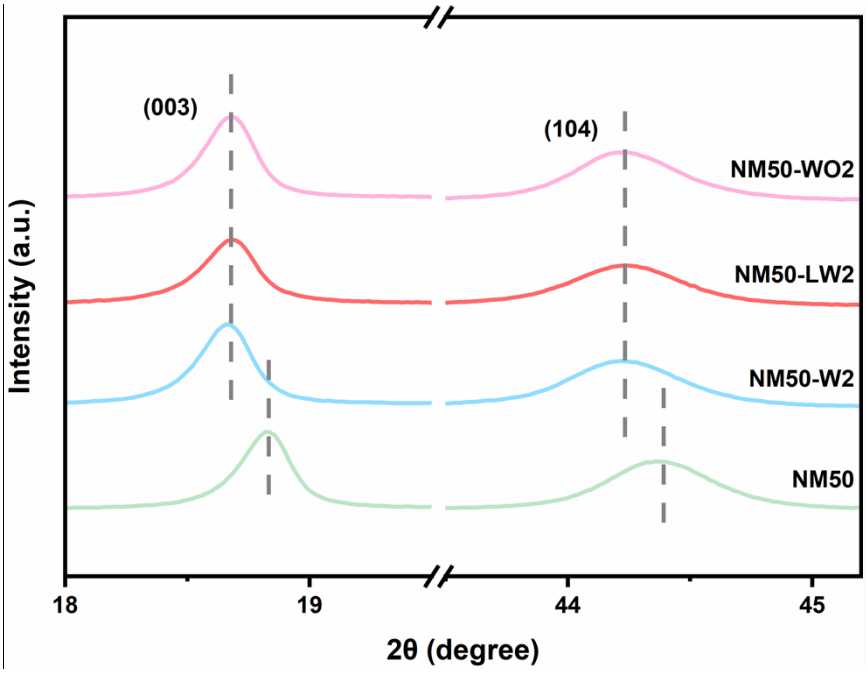

Fig. S3 Enlarged (003) and (104) peaks of the XRD pattern for NM50, NM50-W2, NM50-LW2 and NM50-WO2.

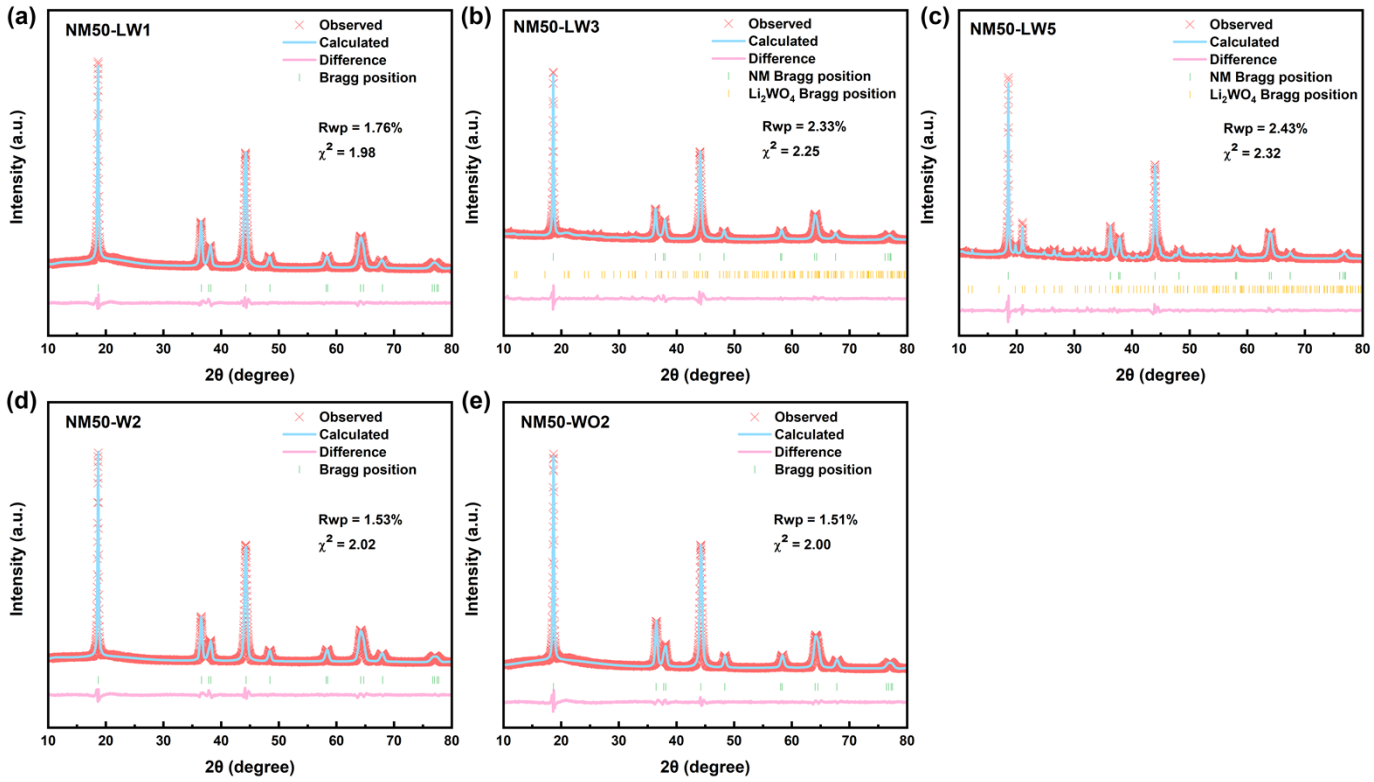

Fig. S4 XRD pattern and corresponding Rietveld refinement results of NM50-LW1 (a), NM50-LW3 (b), NM50-LW5 (c), NM50-W2 (d), and NM50-WO2 (e).

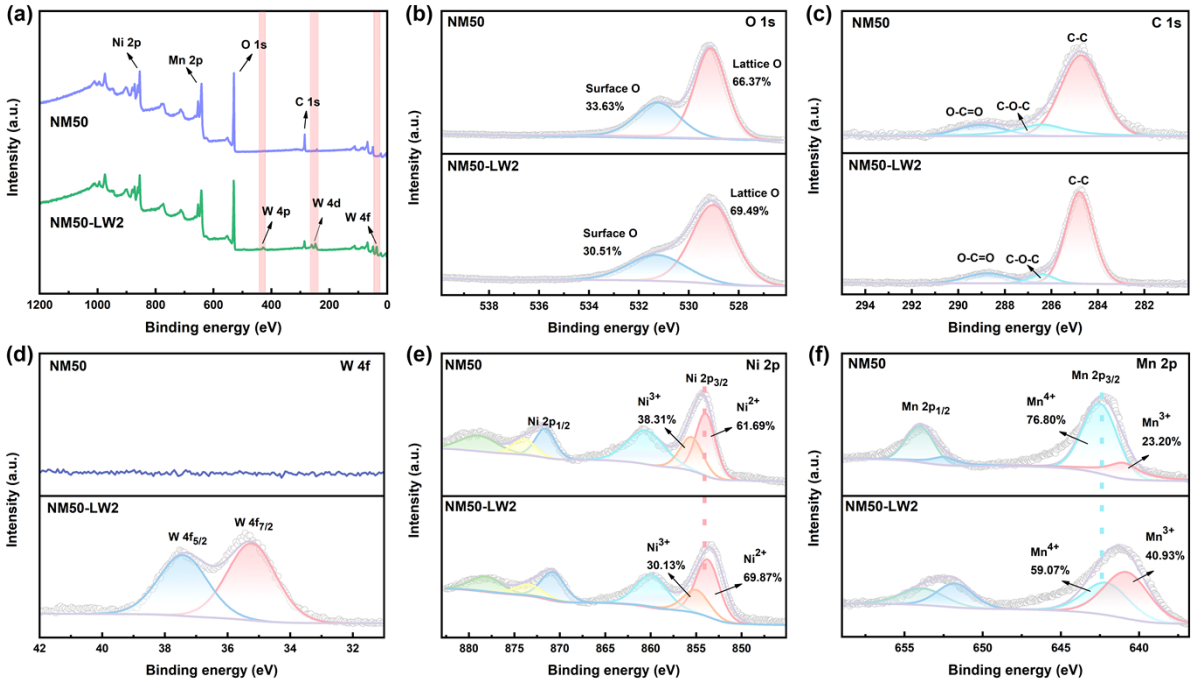

Fig. S5 (a) XPS full spectrum of NM50 and NM50-LW2; (b~f) O 1*s* (b), C 1*s* (c), W 4*f* (d), Ni 2*p* (e) and Mn 2*p* (f) profiles of NM50 and NM-LW2.

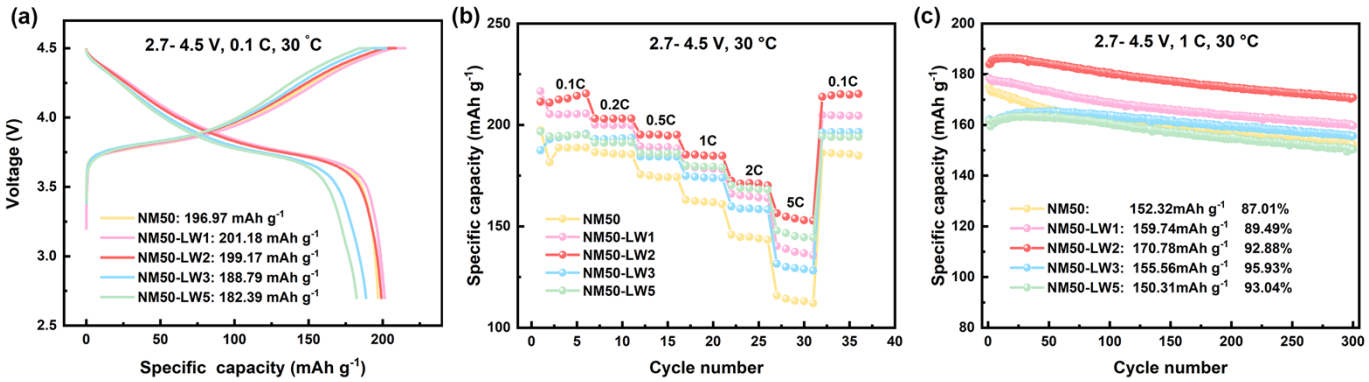

Fig. S6 The initial charging/discharging curves (a), rate capacity (b), cycling performance (c) of NM50, NM50-LW1, NM50-LW2, NM50-LW3 and NM50-LW5 in the potential of 2.7-4.5 V at 0.1 C and 30 °

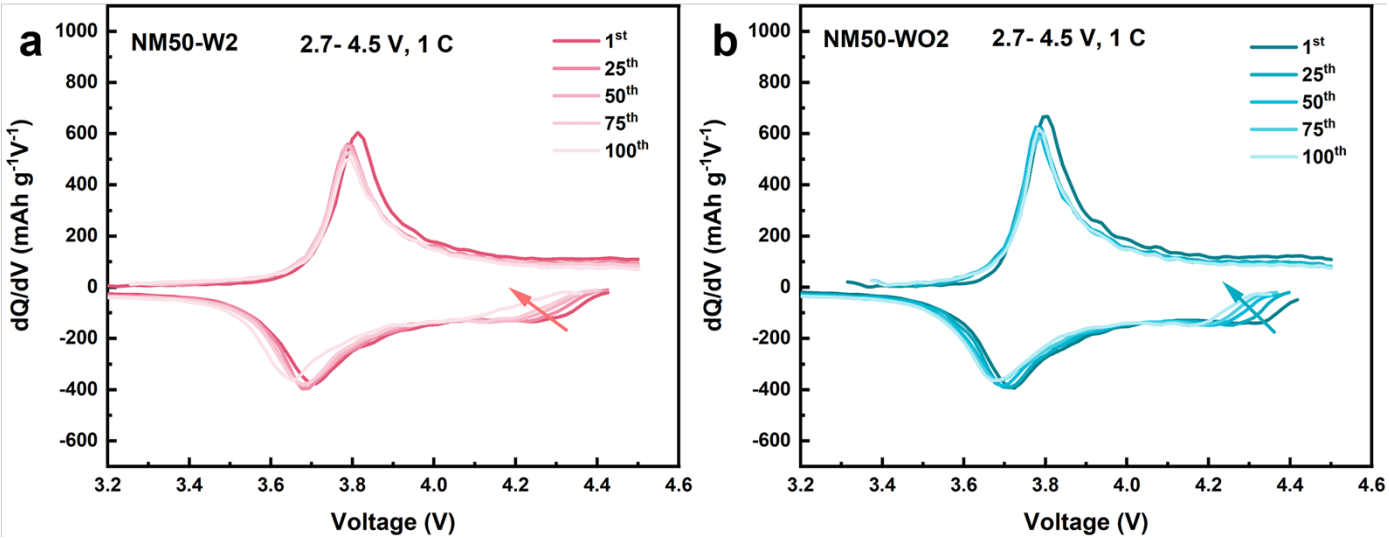

Fig. S7 (a) dQ/dV curves of NM50-W2; (b) dQ/dV curves of NM50-WO2.

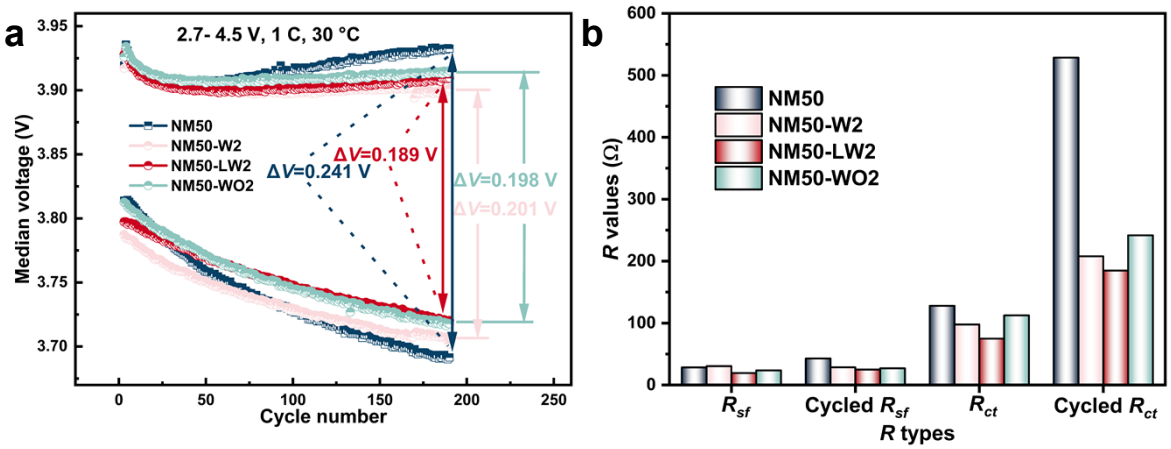

Fig. S8 (a) The median voltage charging/discharging curves of NM50, NM50-W2, NM50-LW2 and NM50-WO2 electrode. (b) EIS Fitting results of NM50, NM50-W2, NM50-LW2 and NM50-WO2 after one cycle and 100 cycles.

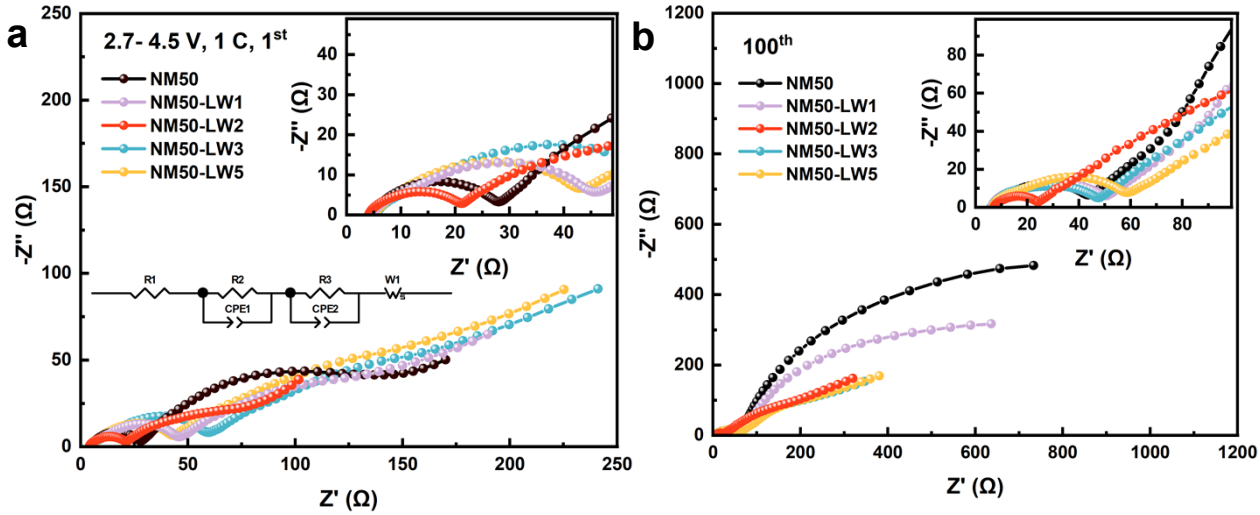

Fig. S9 Nyquist plots of NM50, NM50-LW1, NM50-LW2, NM50-LW3, and NM50-LW2 after the one cycle(a) and 100 cycles (b).

Table S1. Crystallographic parameters of NM50, NM50-LW1, NM50-LW2,NM50-LW3 and NM50-LW5 obtained by Rietveld refinement.

Samples	R_{wp}	χ^2	*a*/*b* (Å)	*c* (Å)	*V* (Å^3)	Li^+/Ni^{2+} mixing
NM50	1.42%	1.85%	2.8761	14.2230	101.809	8.6%
NM50-LW1	1.76%	1.98%	2.8736	14.2437	102.186	8.4%
NM50-LW2	1.36%	1.72%	2.8858	14.2583	102.143	7.3%
NM50-LW3	2.33%	2.25%	2.8951	14.2867	103.700	7.6%
NM50-LW5	2.43%	2.32%	2.8983	14.2937	103.981	8.2%
NM50-W2	1.53%	2.02%	2.8795	14.2650	102.430	8.1%
NM50-WO2	1.51%	2.00%	2.8874	14.2875	103.159	8.2%

Table S2 The fitted results of EIS data.

Sample	1st cycle		100th cycle	
	R_{sf} (Ω)	R_{ct} (Ω)	R_{sf} (Ω)	R_{ct} (Ω)
NM50	28.46	127.8	42.81	528.6
NM50-LW1	36.82	123.5	48.62	467.2
NM50-LW2	19.34	74.83	24.88	184.7
NM50-LW3	52.86	139.6	47.62	223.4
NM50-LW5	35.45	119.8	59.87	243.5
NM50-W2	30.38	97.76	28.69	207.8
NM50-WO2	23.52	112.4	26.92	241.6

Table S3. The comparison of the electrochemical performance of the work with reported cathodes with similar composition.

Number	Samples	Rate capability (3C/5C/8C/10C)	Cycling stability (test conditions)	High cut-off voltage	High temperature
1	NCM622-0.5%W[1]	150.2 mAh g^{-1} / 5 C	96.7% / 3.0-4.5 V 1 C 25 ℃ 100 cycles	/	95.65 % / 3.0-4.5 V 1 C 55 ℃ 100 cycles
2	NCM-622-Al_2O_3[2]	152.5 mAh g^{-1} / 8 C	100.06% / 3.0-4.4 V 1 C 25 ℃ 100 cycles	86.69% / 3.0-4.6 V 1 C 25 ℃ 100 cycles	/
3	$LiNi_{0.5}Mn_{0.43}Ti_{0.02}Mg_{0.02}Nb_{0.01}Mo_{0.02}O_2$[3]	/	81.9% / 2.7-4.5 V 1 C 25 ℃ 100 cycles	/	/
4	NCM523-Pr_6O_{11}[4]	116 mAh g^{-1} / 5 C	77.4% / 3.0-4.5 V 2 C 25 ℃ 100 cycles	/	78.5% / 3.0-4.5 V 2 C 60 ℃ 100 cycles
5	NCM523-$LiNbO_3$[5]	128.9 mAh g^{-1} / 10 C	92% / 3.0-4.5 V 1 C 25 ℃ 100 cycles	/	/
6	NCM622-ZrO_2[6]	112.7 mAh g^{-1} / 10 C	79.0% / 2.8-4.5 V 2 C 25 ℃ 100 cycles	/	/
7	NCM622-ZrV_2O_7[7]	96.9 mAh g^{-1} / 5 C	71.0% / 2.7-4.3 V 0.2 C 25 ℃ 500 cycles	/	67.0% / 2.7-4.3 V 0.2 C 55 ℃ 200 cycles
8	NCM622-$Li_3V_2(PO_4)_3$[8]	118.0 mAh g^{-1} / 5 C	85.0% / 3.0-4.3 V 2 C 25 ℃ 200 cycles	/	/
9	NCM622-Al[9]	145.2 mAh g^{-1} / 5 C	95.26% / 3.0-4.3 V 2 C 25 ℃ 100 cycles	/	/
10	NCM622-Ta[10]	145 mAh g^{-1} / 5 C	83.6% / 3.0-4.5 V 1 C 25 ℃ 100 cycles	/	/
11	$Li_{1.2}Mn_{0.56}Ni_{0.16}Co_{0.08}O_2$-W[11]	125 mAh g^{-1} / 5 C	/	83.2% / 2.5-4.6 V 0.5 C 25 ℃ 200 cycles	/
12	$LiNi_{0.83}Co_{0.07}Mn_{0.1}O_2$-WB[12]	155 mAh g^{-1} / 5 C	93.2% / 2.7-4.3 V 1 C 25 ℃ 200 cycles	/	/
13	$LiNi_{0.9}Mn_{0.1}O_2$-W[13]	182.1 mAh g^{-1} / 5 C	90.1% / 2.8-4.5 V 1 C 25 ℃ 100 cycles	/	
14	W-NA96[14]	185.9 mAh g^{-1} / 10 C	91.5% / 2.7-4.3 V 1 C 30 ℃ 100 cycles	82.7% / 2.7-4.5 V 1 C 30 ℃ 100 cycles	/
15	$LiNi_{0.92}Co_{0.04}Mn_{0.04}O_2$-W[15]	159.1 mAh g^{-1} / 5 C	93.97% / 2.8-4.3 V 0.5 C 25 ℃ 100 cycles	/	/

16	$LiNi_{0.90}Co_{0.04}Mn_{0.04}O_2$-W[16]	152.0 mAh g^{-1} / 3 C	82.1% / 3.0-4.3 V 1 C 25 ℃ 100 cycles	/	/
17	$LiNi_{0.895}Co_{0.04}Mn_{0.03}Al_{0.03}W_{0.005}O_2$[17]	/	95.0% / 2.8-4.3 V 0.5 C 25 ℃ 100 cycles	/	/
18	$LiNi_{0.885}Co_{0.10}Al_{0.015}O_2$-W[18]	/	93.6% / 2.7-4.3 V 0.5 C 30 ℃ 100 cycles	/	/
19	$LiNi_{0.88}Co_{0.09}Al_{0.03}O_2$-W[19]	146.2 mAh g^{-1} / 5 C	95.2% / 2.8-4.3 V 1 C 25 ℃ 100 cycles	/	/
20	$LiNi_{0.8}Co_{0.1}Mn_{0.1}O_2$-W[20]	165.5 mAh g^{-1} / 5 C	88.4% / 3.0-4.3 V 1 C 25 ℃ 100 cycles	72.4% / 3.0-4.5 V 1 C 25 ℃ 100 cycles	49.6% / 3.0-4.5 V 1 C 55 ℃ 100 cycles
Our work	**$LiNi_{0.5}Mn_{0.5}O_2$**	**112.1 mAh g^{-1} / 5 C**	**152.32 mAh g^{-1} (87.01%) / 2.7-4.5 V 1 C 30 ℃ 300 cycles**	**164.41 mAh g^{-1} (88.39%) / 2.7-4.6 V 1 C 30 ℃ 200 cycles**	**161.21 mAh g^{-1} (85.10%) / 2.7-4.5 V 1 C 50 ℃ 300 cycles**
	$LiNi_{0.49}Mn_{0.49}W_{0.02}O_2$	**134.8 mAh g^{-1} / 5 C**	**162.77 mAh g^{-1} (91.67%) / 2.7-4.5 V 1 C 30 ℃ 300 cycles**	**172.81 mAh g^{-1} (90.81%) / 2.7-4.6 V 1 C 30 ℃ 200 cycles**	**170.54 mAh g^{-1} (88.59%) / 2.7-4.5 V 1 C 50 ℃ 300 cycles**
	$0.98LiNi_{0.5}Mn_{0.5}O_2 \cdot 0.02WO_3$	**152.1 mAh g^{-1} / 5 C**	**165.76 mAh g^{-1} (91.84%) / 2.7-4.5 V 1 C 30 ℃ 300 cycles**	**171.10 mAh g^{-1} (90.05%) / 2.7-4.6 V 1 C 30 ℃ 200 cycles**	**166.40 mAh g^{-1} (86.07%) / 2.7-4.5 V 1 C 50 ℃ 300 cycles**
	$0.98LiNi_{0.5}Mn_{0.5}O_2 \cdot 0.02Li_2WO_4$	**156.5 mAh g^{-1} / 5 C**	**170.78 mAh g^{-1} (92.88%) / 2.7-4.5 V 1 C 30 ℃ 300 cycles**	**176.47 mAh g^{-1} (91.15%) / 2.7-4.6 V 1 C 30 ℃ 200 cycles**	**178.69 mAh g^{-1} (91.44%) / 2.7-4.5 V 1 C 50 ℃ 300 cycles**

Reference

[1] B. Chu, L. You, G. Li, T. Huang, A. Yu, Revealing the Role of W-Doping in Enhancing the Electrochemical Performance of the $LiNi_{0.6}Co_{0.2}Mn_{0.2}O_2$ Cathode at 4.5 V, ACS Applied Materials & Interfaces 13 (2021) 7308-7316. https://doi.org/10.1021/acsami.0c21501.

[2] Y. Zhang, G. Xia, J. Zhang, D. Wang, P. Dong, J. Duan, Boosting high-voltage cyclic stability of nickel-rich layered cathodes in full-cell by metallurgy-inspired coating strategy, Applied Surface Science 509 (2020) 145380. https://doi.org/10.1016/j.apsusc.2020.145380.

[3] R. Zhang, C. Wang, P. Zou, R. Lin, L. Ma, T. Li, I.-h. Hwang, W. Xu, C. Sun, S. Trask, H.L. Xin, Long-life lithium-ion batteries realized by low-Ni, Co-free cathode chemistry, Nature Energy 8 (2023) 695-702. https://doi.org/10.1038/s41560-023-01267-y.

[4] G. Zhao, Y. Huang, W. Zhang, J. Gao, C. Xu, L. Shen, P. Lv, Y. Lin, Z. Huang, J. Li, Pr6O11 interfacial engineering toward high-performance NCM523, Chemical Engineering Journal 441 (2022) https://doi.org/10.1016/j.cej.2022.135929.

[5] H. Yu, S. Wang, Y. Hu, G. He, L.Q. Bao, I.P. Parkin, H. Jiang, Lithium-conductive LiNbO3 coated high-voltage $LiNi_{0.5}Co_{0.2}Mn_{0.3}O_2$ cathode with enhanced rate and cyclability, Green Energy & Environment 7 (2022) 266-274. https://doi.org/10.1016/j.gee.2020.09.011.

[6] L. Yao, F. Liang, J. Jin, B.V.R. Chowdari, J. Yang, Z. Wen, Improved electrochemical property of Ni-rich $LiNi_{0.6}Co_{0.2}Mn_{0.2}O_2$ cathode via in-situ ZrO_2 coating for high energy density lithium ion batteries, Chemical Engineering Journal 389 (2020) https://doi.org/10.1016/j.cej.2020.124403.

[7] W. Liu, X. Li, D. Xiong, Y. Hao, J. Li, H. Kou, B. Yan, D. Li, S. Lu, A. Koo, K. Adair, X. Sun, Significantly improving cycling performance of cathodes in lithium ion batteries: The effect of Al_2O_3 and $LiAlO_2$ coatings on $LiNi_{0.6}Co_{0.2}Mn_{0.2}O_2$, Nano Energy 44 (2018) 111-120. https://doi.org/10.1016/j.nanoen.2017.11.010.

[8] D. Wang, Q. Yan, M. Li, H. Gao, J. Tian, Z. Shan, N. Wang, J. Luo, M. Zhou, Z. Chen, Boosting the cycling stability of Ni-rich layered oxide cathode by dry coating of ultrastable $Li_3V_2(PO_4)_3$ nanoparticles, Nanoscale 13 (2021) 2811-2819. https://doi.org/10.1039/D0NR08305D.

[9] R. Zhang, Y. Zheng, Z. Yao, P. Vanaphuti, X. Ma, S. Bong, M. Chen, Y. Liu, F. Cheng, Z. Yang, Y. Wang, Systematic Study of Al Impurity for NCM622 Cathode Materials, ACS Sustainable Chemistry & Engineering 8 (2020) 9875-9884. https://doi.org/10.1021/acssuschemeng.0c02965.

[10] B. Chu, S. Liu, L. You, D. Liu, T. Huang, Y. Li, A. Yu, Enhancing the Cycling Stability of Ni-Rich $LiNi_{0.6}Co_{0.2}Mn_{0.2}O_2$ Cathode at a High Cutoff Voltage with Ta Doping, ACS Sustainable Chemistry & Engineering 8 (2020) 3082-3090. https://doi.org/10.1021/acssuschemeng.9b05560.

[11] J. Meng, L. Xu, Q. Ma, M. Yang, Y. Fang, G. Wan, R. Li, J. Yuan, X. Zhang, H. Yu, L. Liu, T. Liu, Modulating Crystal and Interfacial Properties by W-Gradient Doping for Highly Stable and Long Life Li-Rich Layered Cathodes, Advanced Functional Materials 32 (2022) 2113013. https://doi.org/10.1002/adfm.202113013.

[12] Q. Zhang, Q. Deng, W. Zhong, J. Li, Z. Wang, P. Dong, K. Huang, C. Yang, Tungsten Boride Stabilized Single-Crystal $LiNi_{0.83}Co_{0.07}Mn_{0.1}O_2$ Cathode for High Energy Density Lithium-Ion Batteries: Performance and Mechanisms, Advanced Functional Materials 33 (2023) https://doi.org/10.1002/adfm.202301336.

[13] X. Wang, B. Zhang, Z. Xiao, L. Ming, M. Li, L. Cheng, X. Ou, Enhanced rate capability and mitigated capacity decay of ultrahigh-nickel cobalt-free $LiNi_{0.9}Mn_{0.1}O_2$ cathode at high-voltage by selective tungsten substitution, Chinese Chemical Letters 34 (2023) 107772. https://doi.org/10.1016/j.cclet.2022.107772.

[14] Y. Cheng, X. Zhang, Q. Leng, X. Yang, T. Jiao, Z. Gong, M.-S. Wang, Y. Yang, Boosting electrochemical performance of Co-free Ni-rich cathodes by combination of Al and high-valence elements, Chemical Engineering Journal 474 (2023) https://doi.org/10.1016/j.cej.2023.145869.

[15] D. Gao, Y. Huang, H. Dong, C. Li, C. Chang, Atomic Horizons Interpretation on Enhancing Electrochemical Performance of Ni-Rich NCM Cathode *via* W Doping: Dual Improvements in Electronic and Ionic Conductivities from DFT Calculations and Experimental Confirmation, Small 19 (2022) https://doi.org/10.1002/smll.202205122.
[16] H. Feng, Y. Xu, Y. Zhou, J. Song, J. Yang, Q. Tan, The Y^{3+} and W^{6+} co-doping into Ni-rich Co-free single-crystal cathode $LiNi_{0.9}Mn_{0.1}O_2$ for achieving high electrochemical properties in lithium-ion batteries, Journal of Alloys and Compounds 976 (2024) https://doi.org/10.1016/j.jallcom.2023.173043.
[17] J. Yang, D. Gao, D. Zhang, C. Chang, Effect of dual improved electronic and cationic conductivity via W doping on cyclability and rate performance of $LiNi_{0.90}Co_{0.04}Mn_{0.03}Al_{0.03}O_2$ cathode for rechargeable LIBs, Journal of Energy Storage 63 (2023) https://doi.org/10.1016/j.est.2023.107088.
[18] U.-H. Kim, N.-Y. Park, G.-T. Park, H. Kim, C.S. Yoon, Y.-K. Sun, High-Energy W-Doped $Li[Ni_{0.9}5Co_{0.04}Al_{0.01}]O_2$ Cathodes for Next-Generation Electric Vehicles, Energy Storage Materials 33 (2020) 399-407. https://doi.org/10.1016/j.ensm.2020.08.013.
[19] R. Zhang, H. Qiu, Y. Zhang, Enhancing the Electrochemical Performance of Ni-Rich $LiNi_{0.88}Co_{0.09}Al_{0.03}O_2$ Cathodes through Tungsten-Doping for Lithium-Ion Batteries, Nanomaterials 12 (2022) 729. https://doi.org/10.3390/nano12050729.
[20] Z. Zhu, A. Gao, Y. Liang, F. Yi, T. Meng, J. Ling, J. Hao, D. Shu, Dual-Functional Tungsten Boosted Lithium-Ion Diffusion and Structural Integrity of $LiNi_{0.8}Co_{0.1}Mn_{0.1}O_2$ Cathodes for High Performance Lithium-Ion Batteries, ACS Sustainable Chemistry & Engineering 10 (2022) 50-60. https://doi.org/10.1021/acssuschemeng.1c04076.